Semesta Teknika
Vol. 28, No. 1, 90 - 102, May 2025
DOI: https://doi.org/10.18196/st.v28i1.25116

Numerical study of fluid flow characteristics across a lens wind turbine with vortex generators

Lohdy Diana*, Joke Pratilastiarso, Arrad Ghani Safitra, Muhammad Ricky Ariza
Department of Power Plant Engineering, Politeknik Elektronika Negeri Surabaya

Jl. Raya ITS, Sukolilo, Surabaya, Indonesia

* Corresponding author email: lohdydiana@pens.ac.id

Keywords:
lens; brim; vortex generator; wind turbine

Abstract
Indonesia still needs the development of wind turbine technology to increase the utilization of wind potential. This research will design a wind farm using Lens Wind Turbine with the addition of a vortex generator on the brim surface (LWTvg). The purpose of this research is to produce Lens Wind Turbine (LWTvg) to achieve Green Economy. The vortex generators are put in brim surface with ratio variations z/h=4.5, z/h=2.5, and z/h=0.5. This research uses simulation method to analyze fluid characteristics. The simulation result shows that based on air velocity contour the LWTvg z/h=0.5 has higher air velocity when through the turbine than other variations. The fluid characteristics for air velocity, air pressure, and performance coefficient in top line and middle line are similar but the phenomena are different in bottom line. The number of vortex generators can intensify changes in wind flow velocity around the wind turbine.

INTRODUCTION

At the Indonesia Economic Outlook 2023 seminar, Director General of New, Renewable Energy and Energy Conservation (EBTKE) said the electricity demand in Indonesia has reached 1,172 kWh/capita and will continue to rise along with Indonesia's economic growth which is targeted to reach 5.3% in 2023. For this reason, additional generating capacity from new renewable energy (EBT) is needed. As Indonesia's commitment to contribute to reducing energy sector emissions by 358 million tons of CO2 in 2030" (DAVOS & Dirjen EBTKE, 2023). Based on data from the Ministry of Energy and Mineral Resources in 2021, in Indonesia Bayu or wind energy is ranked second with a potential of 155 Gigawatts but its utilization is still 0.15 Gigawatts (Kementrian ESDM, 2022). This shows that Indonesia still needs the development of wind turbine technology to increase the utilization of wind potential in Indonesia and reduce fossil energy dependence. The development of wind turbine technology is one way to achieve Green Economy and energy independence, especially in 3T areas in Indonesia and in urban areas with low wind velocitys. Many wind turbine studies have been conducted to produce the best performance (Pratilastiarso et al., 2018; Chen & Shiah, 2018). However, one interesting wind turbine design is the Lens Wind Turbine (LWT) which is claimed to have 2-5 times higher performance than conventional turbines in locations with low wind velocitys. One of the variations added to wind turbines, especially on the blades, is the splitted winglet. This additional variation is an adaptation of the latest aircraft. The advantage of using this typical winglet on an airplane is to increase the lift coefficient and decrease the drag coefficient. The function of the splitted winglet on the wind turbine blade is to minimize the backflow at the blade tip. The expectation of this research is that the turbine will get better performance. Comparing turbines with blades without winglets, with winglets and with split winglets. The turbine with blades without winglets gave the best performance among all turbine variations. When the airflow hits the turbine at 6 m/s, the performance of the turbine without the winglet results in a Cp of about 5.2E-1. With the same airflow velocity, the turbine with winglet and split winglet produced Cp of about 4.7E-1 and 2.1E-1 (Pratilastiarso et al., 2018). A wind lens is a new type of wind power system that consists of a simple

edged ring structure that surrounds the rotor, causing more wind to pass through the turbine. Wind lens turbines can produce 2-5 times the power of existing wind turbines given the same rotor diameter and inlet wind velocity. This fluid dynamic effect is also effective in water. The research has developed a 1-3 kW wind lens turbine and a 100 kW wind lens turbine. In addition to the increased output power, wind lens turbines are also quiet. The technology is now being used in offshore experiments with an 18-meter-diameter hexagonal buoy installed off the coast of Hakata Bay in Fukuoka City. In addition, it is now developing larger-sized Wind lens turbines through a multi-rotor design consisting of multiple Wind lens turbines in the same vertical plane to realize greater total power output (Ohya et al., 2017). Horizontal axis wind turbine (HAWT) applications are mainly used for large wind energy capacity, and that is undoubtedly a problem for applications at low velocity potential. However, developments related to performance improvement for small-scale applications are still being studied, one of which is winglet blades. The application of winglets on aircraft provides an advantage in reducing induced drag, leading to an increase in lift. Based on this, the use of winglets on HAWT is an innovation that needs to be studied to maximize its performance. In the study, the effect of winglet blades with the configuration of the number of blades and pitch angle was tested for its effect on wind velocitys of 1.5 m/s to 5 m/s. In the results of the study, it can be seen that increasing the pitch angle and wind velocity affects the energy produced. In addition, it was found that increasing the number of turbine blades would also increase energy and performance. The results showed that the performance of the turbine with four winglet blades was able to produce the highest power, power coefficient (Cp), and tip velocity ratio (TSR) of 11.34 Watt, 0.313 and 3.57, respectively (Wijayanto et al., 2021). The research used the Computational Fluid Dynamics method, the simulation results were carried out in two dimensions. The simulation results show that the lowest mass flow rate value is owned by a turbine without a brim or with a lens, then the second position of the turbine with a lens is proven to increase the mass flow rate of the fluid. Then the first position is a turbine that uses a lens and there is a brim at the end position has the highest mass flow rate compared to other variations (Prasad et al., 2020). The results showed that the counter-rotating vortex generator (VG) appeared to be more effective than the co-rotating VG in terms of producing a significant increase in glide ratio (maximum 36% at 8 degrees angle of attack). Placing the VG near the trailing edge is more efficient than placing it near the leading edge. When the VGs were shifted towards the trailing edge, the stall angle changed from 10 degrees to 12 degrees, with an increase in peak lift coefficient of 11.44%. It can be concluded that in this hydrofoil, the appearance of the stall phenomenon can be delayed by the addition of VGs (Kundu et al., 2019).

After studying several literature studies, a modified Lens Wind Turbine structure was produced. The Lens Wind Turbine concept is actually not a new thing that has existed since the middle of the 20th century (Ohya et al., 2017; Wijayanto et al., 2021; Rinker et al., 2018; Maizi et al., 2018; Prasad et al., 2020). Research on the impact of wind turbines on open areas has also been carried out (Ellerbrok et a., 2024) as well as for urban areas with low wind velocitys (Pellegrini et al., 2021). However, the concept has not been developed in Indonesia, which has low wind velocitys in urban areas as well as in open areas (Novri, 2021; Saputra, 2021). Lens Wind Turbine is proven to be able to increase the performance of wind turbine performance 2-5 times compared to conventional turbines, reduce noise, and secure the turbine from contact with living things, especially birds and other flying objects (Ohya et al., 2017). The formulation of the Lens Wind Turbine modification problem with the addition of a Vortex Generator (LWTvg) in this study includes: how does the ratio of the vortex generator on the brim surface affect the performance of the Lens Wind Turbine and what are the characteristics of the air flow when passing through the wind turbine in the form of wind flow velocity distribution, wind velocity vector formed, etc. The method of approaching the problem above is to apply a winglet turbine based on previous research, a winglet type wind turbine that produces good performance at low wind velocitys (Wijayanto et al., 2021). Measuring the test results using calibrated measuring instruments so that the results are valid (Rinker et al., 2018). Modifying the turbine structure to reduce noise (Maizi et al., 2018). The focus of various studies is on improving wind turbine performance through methods such as the use of shrouds and brims, as well as design optimization using CFD simulations. One study shows that adding a cycloidal-profile shroud to a wind turbine can increase the power coefficient by up to 58% compared to turbines without a shroud (Hashem et al., 2022). Another study using a small-scale HAWT model, found that the model with a shroud experienced a 1.52-fold increase in power coefficient compared to the model without a shroud, with results validated through CFD simulations (Al Quraishi et al., 2019). Further efforts to enhance small wind turbine efficiency by adding various brim configurations optimized through CFD, resulting in increased power

and torque in the rotor blades (Darpe et al., 2020). Additionally, analysis of tip vortex trajectories in shrouded wind turbines, indicating that shrouds alter the tip vortex path and increase axial induced velocity at the rotor plane, showing that the classical Prandtl method is not accurate for shrouded turbine analysis and modern blade functions are required for more precise analysis (Silva et al., 2024).

The novelty of this research is to modify the previously existing Lens Wind Turbine (LWT) into LWTvg, the novelty includes: winglet wind turbines will be installed inside the brim, wiglet wind turbines are proven to have better performance when compared to turbines without winglets (Pratilastiarso et al., 2018; Wijayanto et al., 2021), the rear surface of the brim is added a triangular vortex generator that functions as a vortex shadding flow breaker (Hensen et al., 2016; Sikien et al., 2018). The vortex shedding can be reduced by the initially cylindrical support structure will be replaced using an airfoil shape support structure (Gao et al., 2018; Zargar et al., 2022), the manufacture of turbines using composite materials aims to make the turbine sturdy and strong but lightweight (Shomad & Hidayat, 2021). This research will design a wind farm using Lens Wind Turbine with the addition of a vortex generator on the brim surface (LWTvg). The purpose of this research is to produce Lens Wind Turbine (LWTvg) to realize Green Economy. The vortex generators are put in brim surface with ratio variations z/h=4.5, z/h=2.5, and z/h=0.5. This research uses simulation method to analyze fluid characteristic such as velocity distribution, power coefficient.

RESEARCH METHODS

This research uses Computational Fluid Dynamics Method or simulation method with the following steps, the first step creates 3-dimension model of Lens Wind Turbine with Vortex Generator (LWTvg), the swept LWTvg area has diameter of 1500 mm and brim diameter of 1700 mm, the blade winglet has 30 degrees. There are three variations of vortex generator ratio, variation 1: z/h=4.5 has 20 pieces of vortex generators, variation 2: z/h=2.5 has 30 pieces of vortex generators, and variation 3: z/h= 0.5 has 60 pieces of vortex generators, where z = vortex generator center point distance and h = vortex generator height, which has the performance of breaking the flow on the surface [14] as can be seen in Fig 2. The second step determines the boundary condition and creates mesh. The boundary condition can be seen in Fig.1; it consists of a velocity inlet and a pressure outlet. This model has Number of cells 1057006 and triangular mesh type. The third step is to input parameter settings to run the simulation. Computational Fluid Dynamics (CFD) simulation in this study uses the Navier-Stokes equations, specifically the Reynolds-Averaged Navier-Stokes (RANS) model, to analyze the fluid flow across the turbine. This simulation using standard k epsilon as a turbulent model, SIMPLE, second order for discretization, and properties of fluid can be seen in Table 2. The last step extract data or post processing in this step get velocity contour, velocity graph in many positions, and graph of coefficient performance. Grid independence is carried out to determine the good quality of mesh that is used to analyze fluid characteristics. There are five mesh in this process as can be seen in Table 3, based on the table the mesh D is selected as a good mesh. It is because the mesh D is in stable condition, or it has the smallest error of 0.023 %.

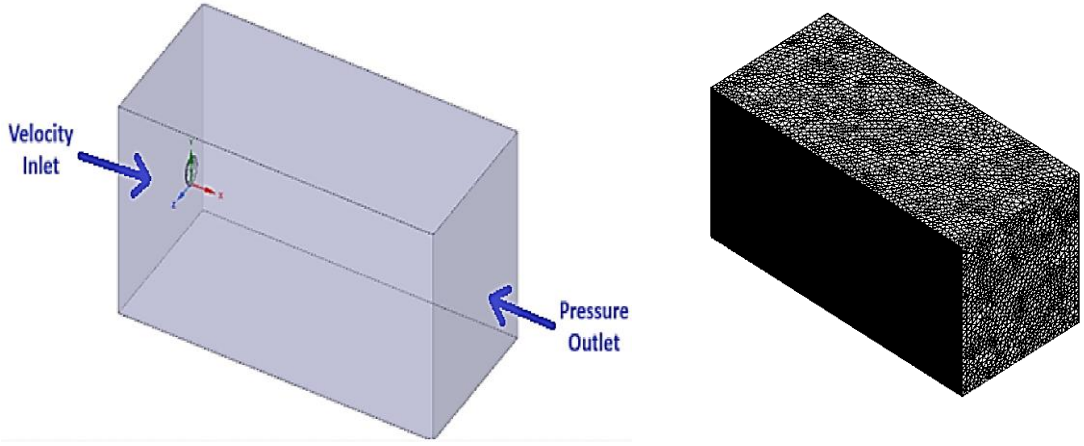

(a) (b)

Figure 1. (a) Boundary Condition and (b)Meshing

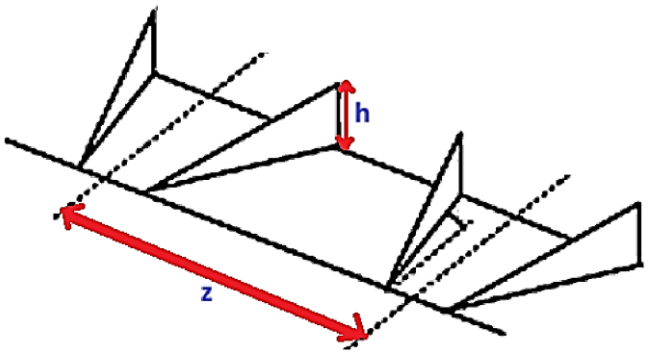

Figure 2. Ratio z/h for Vortex Generator

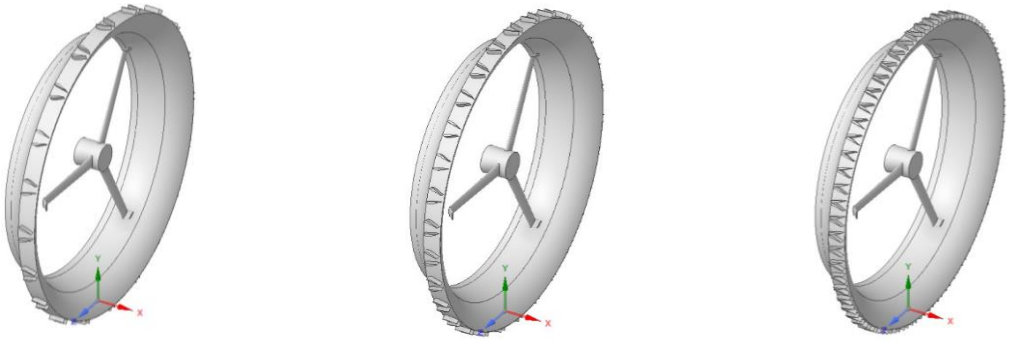

(a) (b) (c)

Figure 3. LWTvg variation (a) z/h=4.5, (b) z/h=2.5, and (c) z/h=0.5

Table 1. Variation of Lens Wind Turbine with Vortex Generators

Variation	z/h	Number of vortex generator
1	4.5	20
2	2.5	30
3	0.5	60

Table 2. Properties of Fluid

Properties	Value	Unit
Air velocity Inlet	3.5	m/s
Air Density	1.225	kg/m^2
Air Viscosity	1.7894e-05	kg/m.s

Table 3. Grid Independency

Mesh	Number of Cells	Air Temperature Outlet (K)	Error (%)
A	550.000	301.10	-
B	760.000	302.02	0.3046
C	970.000	302.11	0.0298
D	290.155	302.18	0.0232
E	1.800.000	302.18	0

RESULTS AND DISCUSSION

The simulation result shows the velocity contour for fluid that flows through the lens wind turbine. Figure 4 shows the fluid velocity contour for z/h=4.5, based on the figure the highest fluid velocity is near the wind turbine hub around 5.05 m/s until 4.04 m/s, it is shown in orange color. This is because no obstacle near the wind turbine hub area. The area is called the swept wind turbine area. The same phenomena happened in other variations z/h=2.5 and z/h=0.5. Figure 4 shows the air velocity distribution around an LWTvg with z/h=4.5, the unique phenomenon observed is the presence of turbulence and vortex formation around the brim, especially in the downstream section. These vortices cause areas of alternating higher and lower wind velocities, which are visible in the color distribution. The red color, indicating a flow velocity of around 4.55m/s to 5.05m/s, is located near the front of the turbine. This indicates an area with very high flow velocity, suggesting that wind velocity increases around the tip of the vortex generators. The yellow to green colors, indicating a flow velocity of 2.02m/s to 3.54m/s, are located around the middle of the brim. These colors suggest that the wind flow begins to slow down as it passes through the brim but remains relatively high due to the influence of the formed vortices. Meanwhile, the blue and cyan colors, with flow velocities of 0.00 to 1.52 m/s, are located behind the brim, indicating areas with low flow velocity. This is likely due to the blockage effect created by the brim and the influence of the vortex generators that impede the wind flow. Overall, the flow pattern formed demonstrates how the vortex generators and brim work together to alter the wind velocity distribution, increasing velocity around the turbine for better efficiency.

Figure 5 shows the velocity distribution around an LWTvg with z/h=2.5, a unique phenomenon observed is the increased wind velocity around the vortex generators and brim, along with the significant vortex formation in the downstream section of the brim. These vortices cause changes in the wind flow pattern, which is evident in the velocity distribution. The red color, indicating wind velocity between 4.55m/s and 5.05m/s, is located around the vortex generators at the front and middle sections of the brim. This color represents areas with very high flow velocity, resulting from the wind acceleration as it passes through the vortex generators. The yellow to green colors, with velocities ranging from 2.02m/s to 4.04 m/s, spread across the middle to the beam rear sections. These colors indicate areas where the flow velocity decreases but remains relatively high, showing how the wind velocity gradually reduces after passing through the vortex generators and brim. The blue and cyan colors, representing wind velocity between 0.00 and 1.51m/s, are seen behind the brim, particularly around the areas where vortices form. These colors indicate regions of low flow velocities, caused by the influence of the vortices and the resistance generated by the brim and vortex generator structure. Overall, this velocity distribution pattern illustrates how the vortex generators and brim collaborate first increase and then decrease the wind flow velocity around the turbine, ultimately affecting the overall performance of the wind turbine.

Figure 6 shows the velocity distribution around an LWTvg with z/h=0.5, a unique phenomenon observed is the increased wind velocity around the vortex generators and brim, along with the formation of significant vortices in the downstream section of the brim. The increased number of vortex generators seems to amplify this effect, with more areas being influenced by changes in the flow pattern. The red color, indicating wind velocity between 4.54m/s and 5.05m/s, is located around the vortex generators at the front of the brim. This color represents areas with very high flow velocity, resulting from the acceleration of wind as it passes through the vortex generators. The yellow to green colors, with velocities ranging from 2.02m/s to 4.04m/s, spread across the middle to the rear sections of the brim. These colors indicate areas where the flow velocity decreases but remains relatively high, showing how the wind velocity gradually reduces after passing through the vortex generators and brim. The blue and cyan colors, representing wind velocity between 0.00 and 1.51m/s, are seen behind the brim, particularly around the areas where vortices form. These colors indicate regions of low flow velocity, caused by the disturbances in the flow created by the vortex generator and brim structure, as well as the influence of the resulting vortices. Overall, this velocity distribution pattern illustrates how increasing the number of vortex generators can intensify changes in wind flow velocity around the wind turbine. The vortex generators and brim work together to first increase and then decrease the wind flow velocity, ultimately affecting the overall performance of the wind turbine. The slowing wind velocity distribution behind the brim is an effect of the vortices generated by the VG, which improves the total efficiency of the turbine (Darpe et al., 2020)

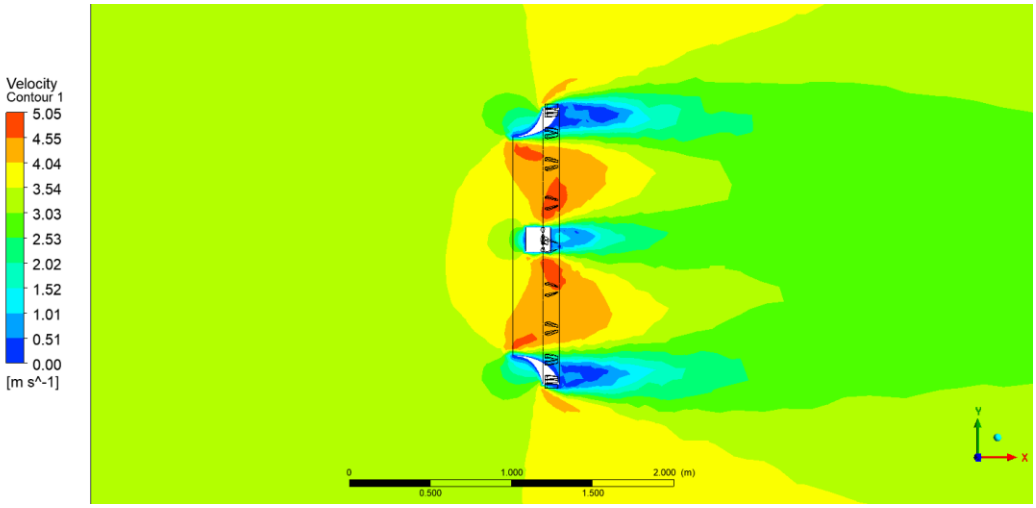

Figure 4. Contour Velocity z/h=4.5 VG 20

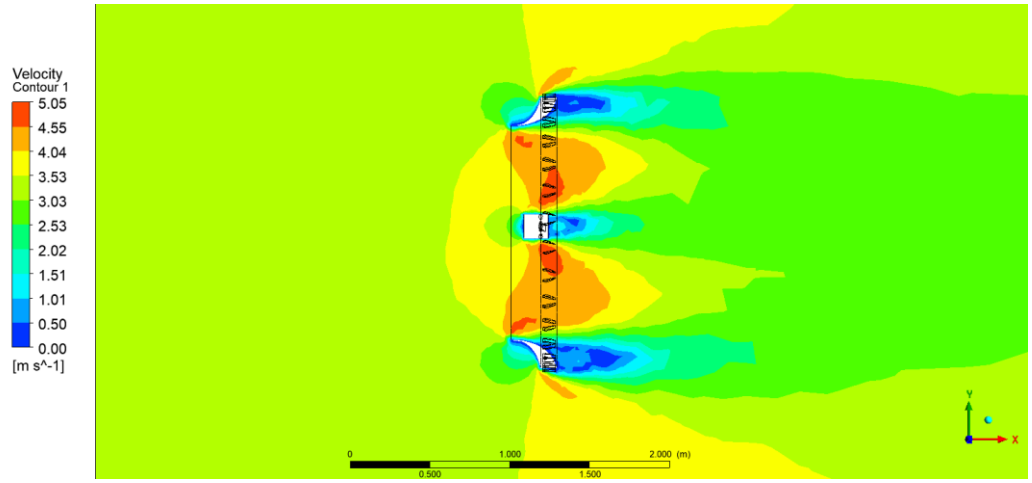

Figure 5. Contour Velocity z/h=2.5 VG 30

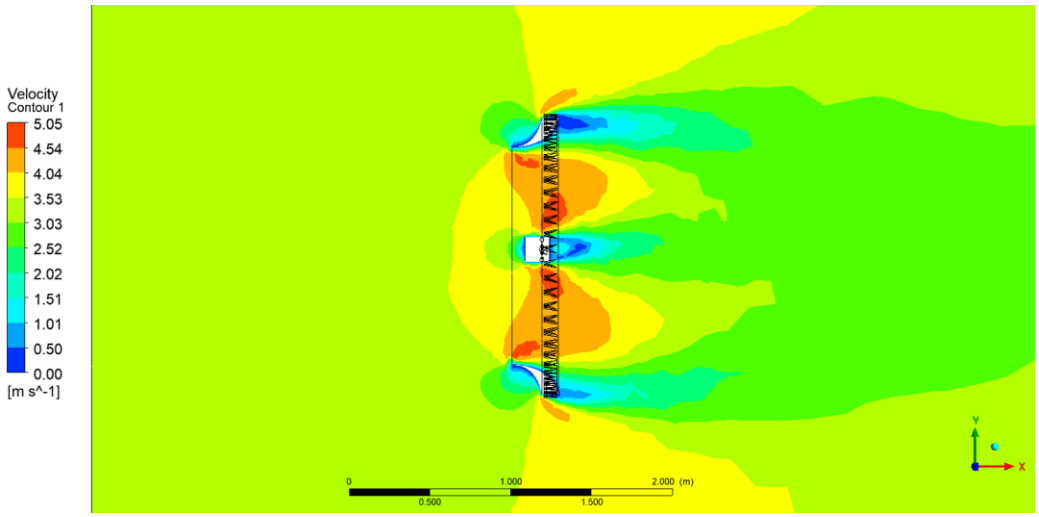

Figure 6. Contour Velocity z/h=0.5 VG 60

Figure 7 (a) illustrates the relationship between position (x) and velocity (m/s) for all variations: z/h=4.5, z/h=2.5, and z/h=0.5 in top line position. At the beginning of the graph, approximately from position x = 0 to

x = 1m, all variations experience a sharp drop in velocity, indicating a drastic deceleration then the velocity increases significant until it stabilizes at around 3.5m/s. This trend is consistent across all variations, although there are slight differences between them as they approach stability. The maximum and minimum values for each variation are as follows: z/h=4.5 top line has a maximum velocity of about 3.7m/s and a minimum of around 0.1m/s. Similarly, both z/h=2.5 top line and z/h=0.5 top line have maximum values of about 3.7 m/s and minimum values around of 0.1m/s. Similar findings regarding wind velocity stability and trends have been reported in prior studies (Darpe et al., 2020). Based on Figure 7 (a), it is evident that the maximum velocity for all variations is nearly the same, at approximately 3.7m/s. There is no significant difference in the maximum and minimum values among the variations. However, upon closer inspection, z/h=0.5 top line appears to be slightly more stable after reaching the maximum velocity, which may give it a slight advantage in terms of velocity stability following the sharp drop. The same phemonema happend to in the middle line position as can be seen in Figure 7 (b) that shows the relationship between position (x) and velocity (m/s) for all variations: z/h=4.5, z/h=2.5, and z/h=0.5 in the niddle line position. Overall, three variations display a similar trend. Initially (around position x = 0 to x = 1m), all variations experience a sharp decrease in velocity, indicating a sudden deceleration. Following this, the velocity increases significant until it stabilizes at around 3.5m/s, with only slight differences between the variations. The maximum and minimum values for each variation are as follows: z/h=4.5 middle line has a maximum velocity of approximately 3.7m/s and a minimum of around 0.1 m/s. The z/h=2.5 middle line variation also has a maximum value of about 3.7m/s and a minimum of around 0.1 m/s, while z/h=0.5 middle line has a maximum of approximately 3.7m/s and a minimum of around 0.1m/s. All these variations show nearly identical maximum values of around 3.7m/s and minimum values of about 0.1 m/s. There is no significant difference between the variations in terms of maximum and minimum values. However, the slight difference in velocity stability after reaching the maximum value may suggest that the z/h=0.5 middle line variation is slightly more stable than the others. This consistent behavior of velocity trends across variations aligns with established theoretical models of flow through turbine systems (Ruifang et al., 2022).

Figure 7 (c) illustrates the relationship between position (x) and velocity (m/s) for for all variations: z/h=4.5, z/h=2.5, and z/h=0.5 in bottom line position. Initially, from position x = 0 to x = 2m, all variations experience a significant increase in velocity, peaking at around 3.6m/s. After reaching this peak, the velocity drops drastically until position x = 5m, followed by small fluctuations before finally stabilizing at around 3.45m/s for all variations. In the range from position x = 10 m to x = 25m, the velocity remains stable with slight differences between the variations. The maximum and minimum values for each variation are as follows: z/h=4.5 bottom line has a maximum velocity of approximately 3.61 m/s and a minimum of around 3.42m/s. The same applies to z/h=2.5 bottom line and z/h=0.5 bottom line each with a maximum value of around 3.61m/s and a minimum of about 3.42m/s. The maximum and minimum velocities of all variations are nearly identical, with similar trend patterns throughout the graph. Although there are slight fluctuations, no variation is significantly higher or lower than the others in terms of maximum and minimum values.

Figure 8 (a) shows the relationship between position (x) and pressure for for all variations: z/h=4.5, z/h=2.5, and z/h=0.5 in top line position. At the beginning of the graph, around position x = 0, all variations show a sharp decrease in pressure. Following this drop, the pressure rises significantly until it stabilizes at around 0. This trend is consistent across all variations, though there are slight differences as they approach stability. The maximum and minimum pressure values for each variation are as follows: z/h=4.5 Top line has a maximum pressure of approximately 7.5Pa and a minimum of around -8.1Pa. Similarly, z/h=2.5 top line and z/h=0.5 top line both have maximum values near 7.5Pa and minimum values around -8.1Pa. The graph indicates that the maximum pressure for all variations is nearly identical, at approximately 12.5Pa. There is no significant difference in the maximum and minimum values among the variations.

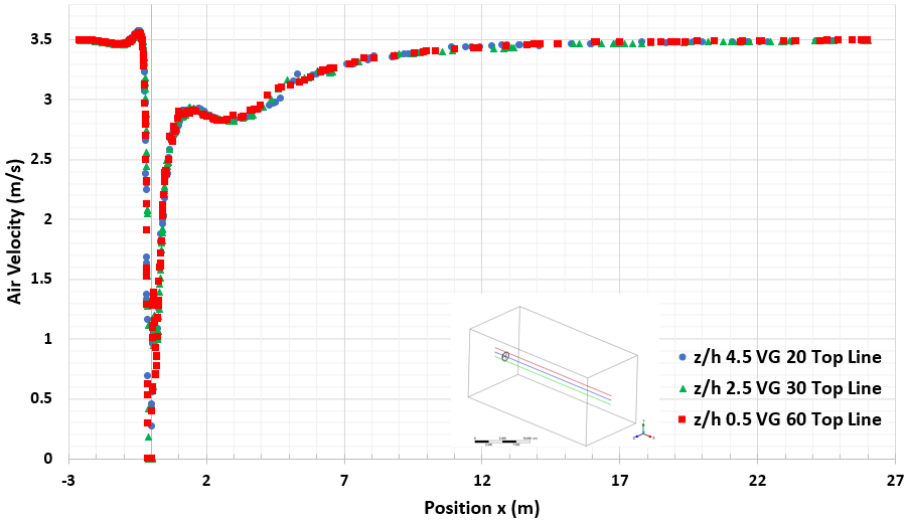

(a)

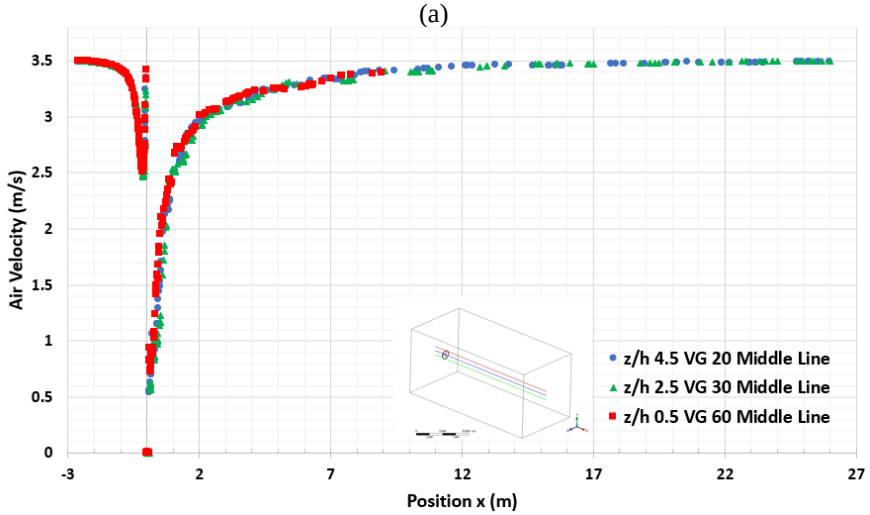

(b)

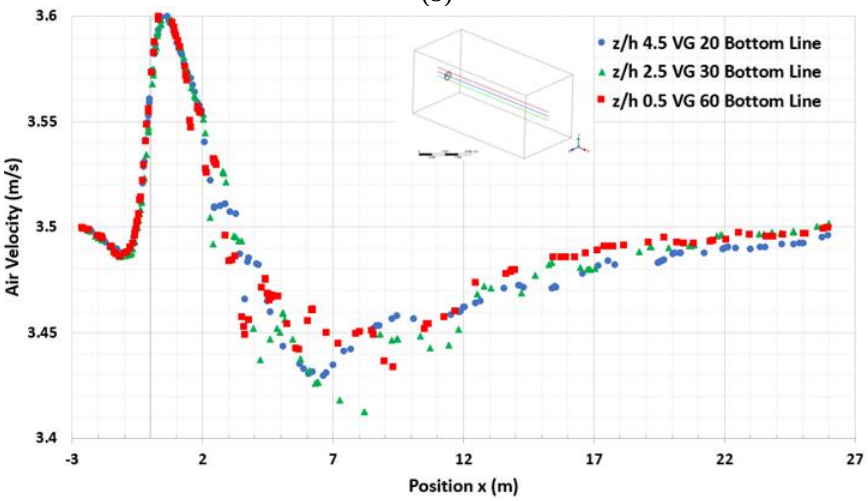

(c)

Figure 7. Air Velocity (a) Top Line Velocity, (b) Middle line Velocity, (c) Bottom line Velocity

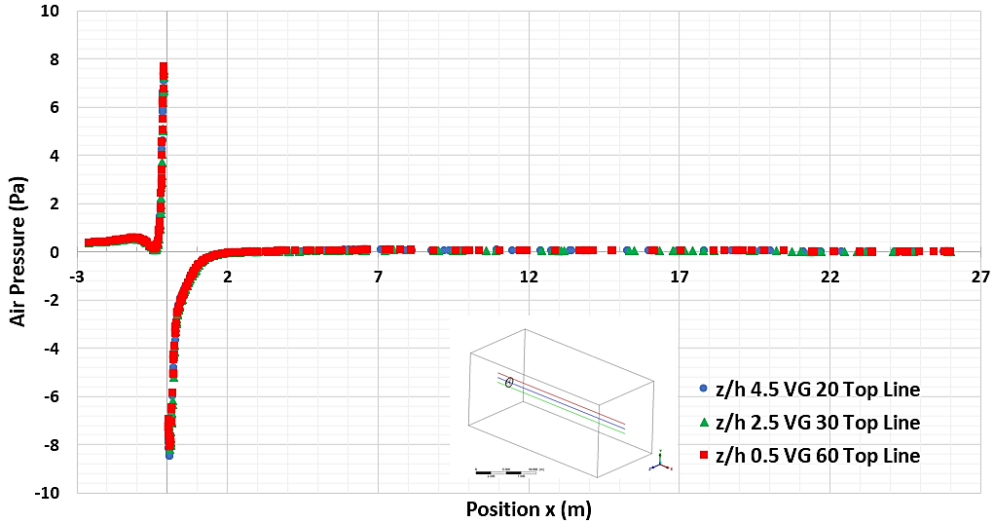

(a)

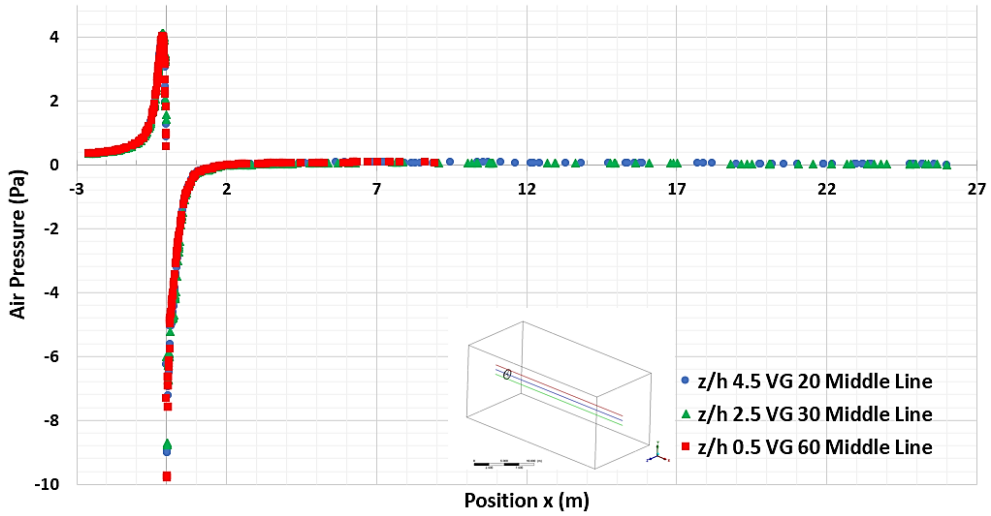

(b)

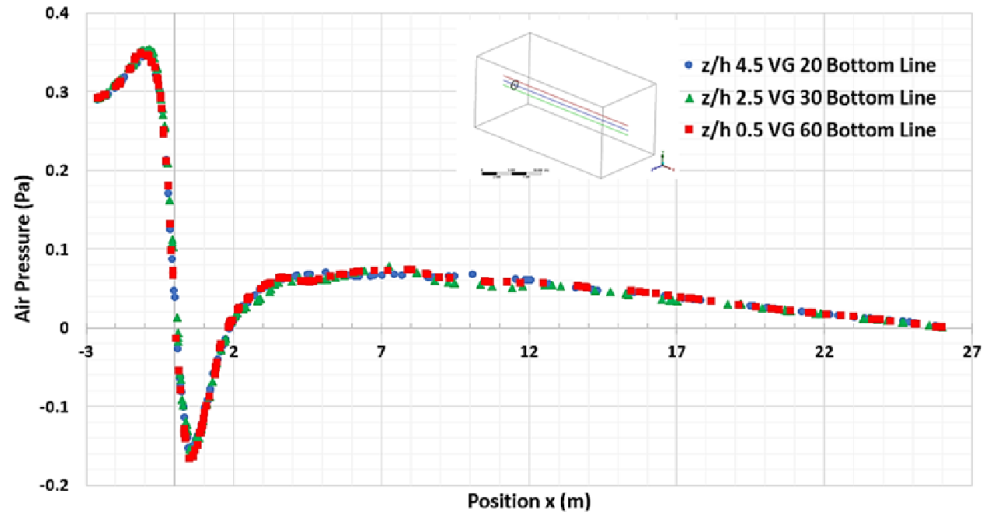

(c)

Figure 8. Air Pressure (a) Top Line Pressure, (b) Top Line Pressure, (c) Bottom line Pressure.

Figure 8 (b) illustrates the relationship between position (x) and pressure for for all variations: z/h=4.5, z/h=2.5, and z/h=0.5 in middle line position, At the start of the graph, around position x = 0, all variations exhibit a sharp drop in pressure. Following this decline, the pressure rises significantly until it stabilizes around 0. This trend is consistent across all variations, though there are slight differences as they approach stability. This behavior aligns with studies that emphasize the role of vortex shedding and pressure redistribution induced by flow dynamics, especially in configurations with differing height ratios (Yan et al., 2019). The maximum and minimum pressure values for each variation are as follows: z/h=4.5 middle line has a maximum pressure of about 4Pa and a minimum of around -9Pa. Similarly, z/h=2.5 middle line and z/h=0.5 middle line both have maximum values of around 6.6. However, the minimum pressure for z/h=2.5 middle line is around -8Pa, while for z/h=0.5 middle line it is around -9.7Pa. The graph shows that the maximum pressure values for all variations are nearly the same, around 6.6Pa. There is no significant difference in the maximum and minimum values among the variations.

Figure 8 (c) shows the relationship between position (x) and pressure for for all variations: z/h=4.5, z/h=2.5, and z/h=0.5 in bottom line position. At the beginning of the graph, from around position x = -1m to x = 0.5m, all variations experience a sharp drop in pressure. After this decrease, the pressure rises significantly until it stabilizes around 0.03Pa. However, at position x = 10m, all variations undergo a slight decline in pressure, continuing until position x = 26m. This trend is similar across all variations, with only minor differences between them. The maximum and minimum pressure values for each variation are as follows: z/h=4.5 bottom line has a maximum pressure of approximately 0.34Pa and a minimum of around -0.15Pa. Similarly, both z/h=2.5 bottom line and z/h=0.5 bottom line has maximum values around 0.34Pa and minimum values around -0.15Pa. This consistent trend is often associated with the redistribution of airflow caused by boundary-layer separation and reattachment, as highlighted in similar simulations on micro-vortex generators for aerodynamic improvement (Yan et al., 2019). The graph indicates that the maximum pressure for all variations is nearly the same, at around 0.15Pa. There is no significant difference in the maximum and minimum values among the variations.

Figure 9 (a) illustrates the relationship between position (x) and CP for for all variations: z/h=4.5, z/h=2.5, and z/h=0.5 in top line position. At the start of the graph, around position x = 0, all variations experience a sharp decline in CP values. After this drop, CP rises significantly until it stabilizes around 0. This trend is consistent across all variations, though there are slight differences as they approach stability. The maximum and minimum CP values for each variation are as follows: z/h=4.5 Top line has a maximum CP value of about 12.5 and a minimum of around -13.5. Similarly, z/h=2.5 top line and z/h=0.5 top line both have maximum values of approximately 12.5 and minimum values around -13.5. The graph indicates that the maximum CP values for all variations are nearly identical, around 12.5, with no significant difference in the maximum and minimum values among the variations.

Figure 9 (b) shows the relationship between position (x) and CP for for all variations: z/h=4.5, z/h=2.5, and z/h=0.5 in middle line position. At the beginning of the graph, around position x = 0, all variations experience a sharp drop in CP. Following this decline, CP rises significantly until it stabilizes around 0. The trend is consistent across all variations, though there are slight differences as they approach stability. The maximum and minimum CP values for each variation are as follows: z/h=4.5 middle line has a maximum CP value of about 6.6 and a minimum of around -14.7. Similarly, z/h=2.5 middle line and z/h=0.5 middle line both have maximum values of approximately 6.6. However, the minimum CP value for z/h=2.5 middle line is around -14.2, while for z/h=0.5 middle line it is around -15.9. The graph indicates that the maximum CP values for all variations are nearly identical at about 6.6, with no significant difference in maximum and minimum values among the variations.

Figure 9 (c) illustrates the relationship between position (x) and CP for for all variations: z/h=4.5, z/h=2.5, and z/h=0.5 in bottom line position. At the beginning of the graph, approximately from position x = -1m to x = 0.5m, all variations show a sharp decline in CP. Following this drop, CP increases significantly, stabilizing around 0.1. However, at position x = 10, all variations experience a slight decline that continues until position x = 26m. The trends are similar across all variations, with only minor differences among them. The maximum and minimum CP values for each variation are as follows: z/h=4.5 bottom line has a maximum CP of about 0.57 and a minimum of around -0.25. Similarly, z/h=2.5 bottom line and z/h=0.5 bottom line both have maximum values of approximately 0.57 and minimum values around -0.25. The graph indicates that the

maximum CP values for all variations are nearly identical at around 0.57, with no significant differences in maximum and minimum values among the variations.

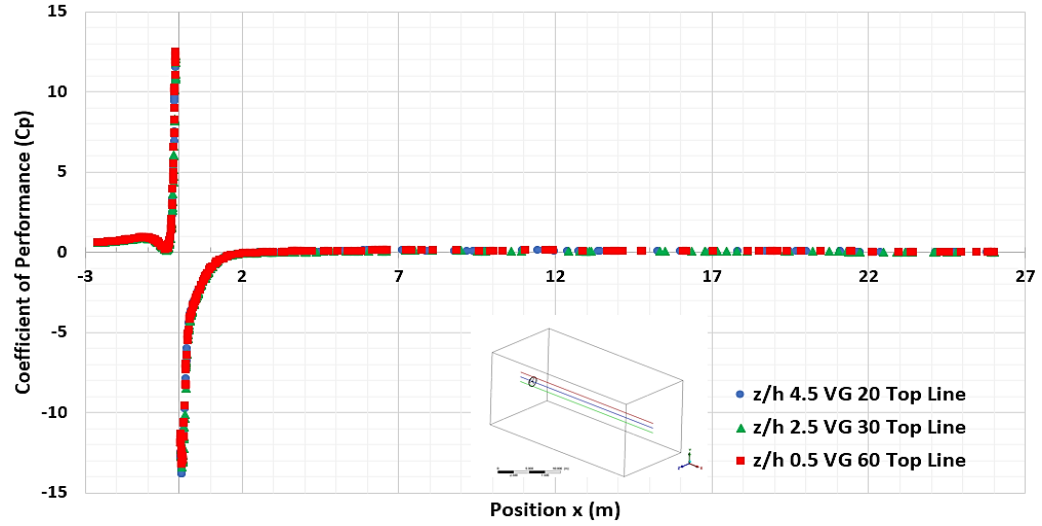

(a)

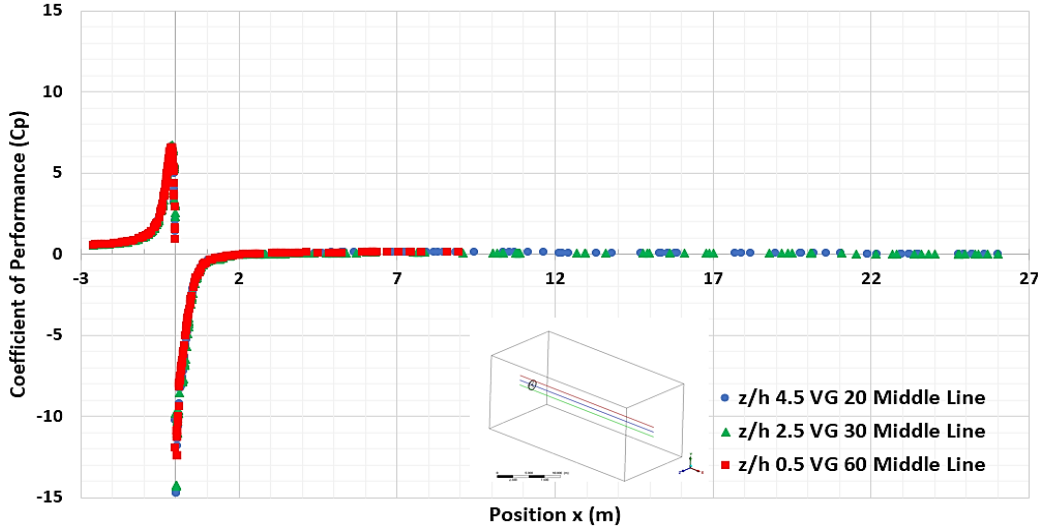

(b)

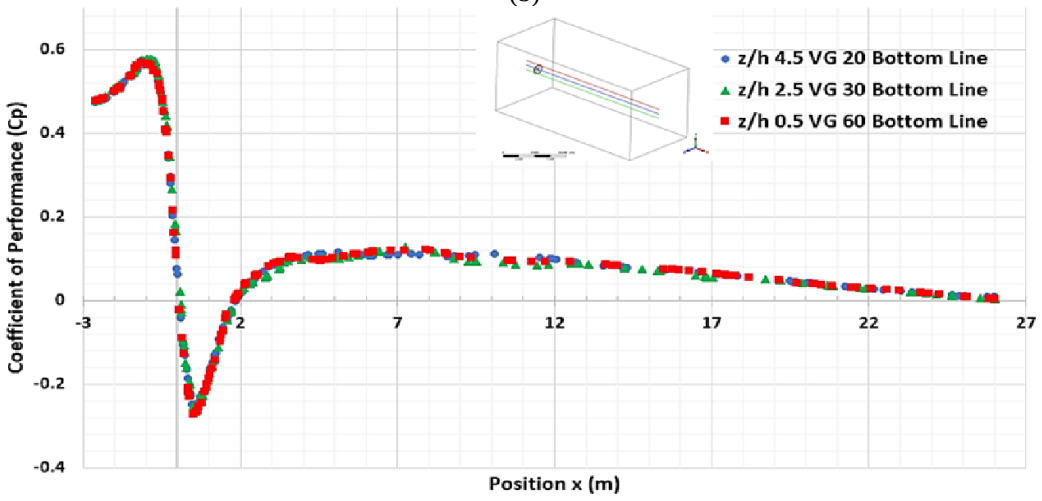

(c)

Figure 9. Coefficient of Performance (a) Top Line CP, (b) Middle line CP, (c) Bottom line CP.

CONCLUSION

Based on air velocity contour the LWTvg z/h=0.5 VG 60 has more high air velocity when through the turbine than other variation. The fluid characteristics for air velocity, air pressure, and performance coefficient in top line and middle line are relative same but the phenomena is different in bottom line. The number of vortex generators can intensify changes in wind flow velocity around the wind turbine. The vortex generators and brim work together to first increase and then decrease the wind flow velocity, ultimately affecting the overall performance of the wind turbine.

REFERENCES

Al-Quraishi, B. A., Asmuin, N. Z., Nemah, M. N., & Salih Meri, A. (2019). Experimental and simulation investigation for performance of a small-scale of bare and shrouded hawt. *International Journal of Mechanical Engineering and Technology, 10*(1), 434-449. http://www.iaeme.com/ijmet/issues.asp?JType=IJMET&VType=10&IType=1

Auliana Rahmawaty, S., Parmita, A. W. Y. P., Laksono, A. D. (2021). Analisa kekuatan tarik dan tekuk pada komposit fiberglas-polyester berpenguat serat gelas dengan variasi fraksi volume serat. *Jurnal Teknik Mesin-ITI, 5*(3), 146-155.

Chen, Y. J., & Shiah, Y. C. (2016). Experiments on the performance of small horizontal axis wind turbine with passive pitch control by disk pulley. *Energies, 9*(5), 353. https://doi.org/10.3390/en9050353

Darpe, M. M., Bandekar, S. K., & Vanjari, S. V. (2020). Design and optimization of a brim augmented wind turbine (wind lens turbine) using CFD. *International Research Journal of Engineering and Technology (IRJET), 7*(4), 962-968.

DAVOS. Dirjen EBTKE. (2023). Dirjen EBTKE Paparkan Pemenuhan Kebutuhan Listrik Indonesia Melalui Pemanfaatan EBT.

Ellerbrok, J. S., Farwig, N., Peter, F., & Voigt, C. C. (2024). Forest bat activity declines with increasing wind velocity in proximity of operating wind turbines. *Global Ecology and Conservation, 49*, e02782. https://doi.org/10.1016/j.gecco.2023.e02782

Gao, Y., Zong, Z., Zou, L., Takagi, S., & Jiang Z. (2018). Numerical simulation of vortex-induced vibration of a circular cylinder with different surface roughnesses. *Marine Structures, 57*, 165-179. https://doi.org/10.1016/j.marstruc.2017.10.007

Hansen, M. O. L., Velte, C. M., Øye, S., Hansen, R., Sørensen, N. N., Madsen J., & Mikkelsen, R. (2016). Aerodynamically shaped vortex generators. *Wind Energy, 19*(3), 563–567. https://doi.org/10.1002/we.1842

Hashem, I., Hafiz, A. A., & Mohamed, M. H. (2022). Characterization of aerodynamic performance of wind-lens turbine using high-fidelity CFD simulations. *Frontiers in Energy, 16*, 661-682. https://doi.org/10.1007/s11708-020-0713-0

KEMENTERIAN ESDM. Media Indonesia. (2022). Potensi EBT di Indonesia Melimpah.

Kundu, P., Sarkar, A., & Nagarajan, V. (2019). Improvement of performance of S1210 hydrofoil with vortex generators and modified trailing edge, Renewable Energy, 142, 643-657. https://doi.org/10.1016/j.renene.2004.148

Maizi, M., Mohamed, M. H., Dizene, R., & Mihoubi, M. C. (2018). Noise reduction of a horizontal wind turbine using different blade shapes. *Renewable Energy, 117*, 242–256. https://doi.org/10.1016/j.renene.2017.10.058

Novri, R. R. (2021). The analisis potensi energi angin tambak untuk menghasilkan energi listrik. *Journal of Research and Education Chemistry, 3*(2), 96. https://journal.uir.ac.id/index.php/jrec/article/view/7165

Ohya, Y., Karasudani T., Nagai, T., & Watanabe, K. (2017). Wind lens technology and its application to wind and water turbine and beyond. *Renewable Energy and Environmental Sustainability, 2*(2). https://doi.org/10.1051/rees/2016022

Pellegrini M., Guzzini A., & Saccani C. (2021). Experimental measurements of the performance of a micro-wind turbine located in an urban area. *Energy Reports*, *7*, 3922–34. https://doi.org/10.1016/j.egyr.2021.05.081

Petrus Sidabutar, S., & Arwinda Setyaningrum, R. (2021). Perancangan bilah inverse taper berbahan styrofoam dengan airfoil naca 4412, *Rotor, 14*(2), 70-74.

Prasad, K. R., Manoj Kumar, V., Swaminathan, G., & Loganathan, G. B. (2020). Computational investigation and design optimization of a duct augmented wind turbine (DAWT). *Materials Today: Proceedings*, *22*(3), 1186–1191. https://doi.org/10.1016/j.matpr.2019.12.116

Pratilastiarso, J., Nugroho, S., Tridianto, E., & Syifa, R. I. (2018). Experimental study on horizontal axis wind turbine with splitted winglets. *IOP Conference Series: Earth and Environmental Science*, *105*, 012102. https://doi.org/ 10.1088/1755-1315/105/1/012102

Rinker, J. M., Hansen, M. H., & Larsen, T. J. (2018). Calibrating a wind turbine model using diverse datasets. *Journal of Physics: Conference Series*, *1037*(6), 062026. https://doi.org/10.1088/1742-6596/1037/6/062026.

Ruifang, J., Zhao, Z., Liu, H., Wang, T., Chen, M. J. F., & Wang, D. (2022). Numerical study on the influence of vortex generators on wind turbine aerodynamic performance considering rotational effect. *Renewable Energy*, *186*, 730-741. https://doi.org/10.1016/j.renene.2022.01.026

Saputra, I. (2021). Analisa daya pembangkit listrik pada pesisir Pantai Labu. *Jurnal Ilmiah Mahasiswa Teknik*, *1*(3), 1-13.

Shomad, M. A., & Hidayat, F. R. (2021). Vertical blade fiberglass composite for wind turbine power plant application. Journal of Robotics and Control (JRC), 2(3):148–52. https://doi.org/10.18196/jrc.2369

Sikien, E. R., Abdullah, A., Zulkafli M. F., & Rahim, M. Z. (2018). The effects of vortex shedding on the aerodynamic performance of airfoils. *ARPN Journal of Engineering and Applied Sciences, 13*(24), 9344-9351.

Silva, P. A. S. F., Tsoutsanis, P., Vaz, J. R. P., & Macias, M. M. (2024). A comprehensive CFD investigation of tip vortex trajectory in shrouded wind turbines using compressible RANS solver. *Energy*, *294*, 130929. https://doi.org/10.1016/j.energy.2024.130929

Wijayanto, D. S., Soenarto, S., Triyono, M. B., & Sangidzun, A. (2021). Experimental study of the effect of winglets on horizontal wind turbine (HAWT) performance. *International Energy Journal*, *21*(3), 375-384.

Yan Y., Eldad A., John W., & Jiahuan C. (2019). CFD analysis for the performance of micro-vortex generator on aerofoil and vertical axis turbine. *Journal of Renewable and Sustainable Energy, 11*(4), 043302. https://doi.org/10.1063/1.5110422

Zargar, O. A., Lin, T., Zebua, A. G., Lai, T. J., Shih, Y. C., Hu, S. C., & Leggett, G. (2022) The effects of surface modification on aerodynamic characteristics of airfoil DU 06 W 200 at low Reynolds numbers. *International Journal of Thermofluids, 16*, 100208. https://doi.org/10.1016/j.ijft.2022.100208